Remission spectroscopy resolves the mode of action of bedaquiline within living mycobacteria

Suzanna H Harrison[1,2*], Rowan C Walters[1,2*], Chen-Yi Cheung[3], Roger J Springett[1,2,4], Gregory M Cook[3,5], Morwan M Osman[1,2 † *], James N Blaza[1,2 †]

[1] York Structural Biology Laboratory, Department of Chemistry, University of York, York, YO10 5DD. [2] York Biomedical Research Institute, University of York, York, YO10 5DD. [3] Department of Microbiology and Immunology, University of Otago, Dunedin 9016, New Zealand. [4] Cellspex Ltd, Northamptonshire, UK. [5] School of Biomedical Sciences, Queensland University of Technology, Brisbane, Queensland 4000, Australia.

* These authors contributed equally to the work † To whom correspondence should be addressed: jamie.blaza@york.ac.uk, morwan.osman@york.ac.uk

Abstract

Bedaquiline, an ATP synthase inhibitor, is the spearhead of transformative therapies against drug-resistant *Mycobacterium tuberculosis*. Beyond causing a cellular energetic crisis, different *in vivo* mechanisms of action have been proposed. Here, we apply remission spectroscopy to measure the electron-occupancy of the energy-transducing cytochromes within the mycobacterial and human bioenergetic systems as they power living cells. We find no evidence for bedaquiline's protonophoric or ionophoric uncoupling activity but observe sub-second redirection of electron flux to the cytochrome *bd* oxidase, Cyd, bypassing the respiratory control ATP synthase imposes on the electron transport chain. We find that bedaquiline does not affect human mitochondrial function. Overall, we explain how bedaquiline works, why different models for its action developed, and the mechanisms underlying bedaquiline's synergy in combination regimes.

Abbreviations

BDQ - bedaquiline; CCCP - carbonyl cyanide m-chlorophenyl hydrazone; CCD - charge coupled device; DCCD - N,N′-dicyclohexylcarbodiimide; ETC - electron transport chain; EtOH - ethanol; Hsa - *Homo sapiens*; MDR - multidrug-resistant; MK/MKH_2- menaquinone/menaquinol; Msm - *Mycobacterium smegmatis*; Mtb - *Mycobacterium tuberculosis*; OCR - oxygen consumption rate; PMF - proton motive force; RCF - relative centrifugal force; TB - tuberculosis; P_i- inorganic phosphate

Introduction

Tuberculosis (TB) is the world's worst infectious killer: 1.3 million people die of TB annually, with another 10 million becoming infected (*1*). When approved, bedaquiline was the first new drug in over four decades, and as part of the BPaL regime (bedaquiline, pretomanid, linezolid) it has transformed the treatment of drug-resistant TB. (*2*, *3*). Resistance to bedaquiline is growing rapidly with evidence of bedaquiline-resistant *Mycobacterium tuberculosis* (Mtb) reinfecting new patients (*4*).

Bedaquiline binds to ATP synthase of the oxidative phosphorylation system (*5*). *In vitro* resistance mutants localise to AtpE (the ring-forming 'c' subunit composed of a circular c_9 ring in the F_O membrane domain) (*6*) and bedaquiline immobilised on a column binds to mycobacterial ATP synthase (*7*). The binding site has been confirmed in a 1.7 Å crystallographic map of the isolated c-ring from *Mycobacterium phlei*, and in cryo-EM maps of the full enzyme from *Mycobacterium smegmatis* (Msm) and Mtb (*8–10*). Worryingly, bedaquiline inhibits human ATP synthases *in vitro* (*10*, *11*). When Mtb is exposed to bedaquiline, ATP depletion starts to occur within hours but cell death takes around a week, consistent with metabolic remodelling allowing the cell to survive in a stressed but alive state that is ultimately overwhelmed (*12*). Induced metabolic changes include the bypass of ATP-demanding enzymes such as phosphofructokinase, upregulation of the glyoxylate shunt, and secretion of metabolites such as succinate (*13*).

The electron transport chain (ETC) builds the proton-motive force (PMF) in respiratory organisms, powering ATP synthesis. As ATP synthase consumes the PMF, it imposes respiratory control on the ETC through 'backpressure', the PMF-based 'force' that resists forward catalysis by the ETC, slowing the O_2-consumption rate (OCR). Remarkably, when bedaquiline is placed on cells an increase in OCR is observed, opposite to how an inhibitor of ATP synthase should act (*14–16*). Two proposals were advanced to explain this effect. One is that bedaquiline is itself an ionophore that acts when 'tailgating' ATP synthase; this activity may be either bedaquiline acting as a protonophoric uncoupler (*15*), or an ionophoric uncoupler that interchanges K^+ and H^+ potentials (*16*). The uncoupler proposals were supported by later cryo-EM studies that reported three kinds of binding sites in the F_O domain and that bedaquiline disrupts the physical communication between the ATP synthase F_O and F_1 domains as its concentration increases (*9*). A second proposal is that mycobacteria either lack backpressure or have mechanisms to collapse it, allowing the ETC to run fast even when ATP synthase is inhibited (*14*). A fundamental difficulty in differentiating between these activities is that an increase in OCR can be caused by a collapse in PMF, metabolic changes that increase electron delivery to the chain, or changes in the regulation of enzymes within the ETC. Therefore, studies on intact cells that measure OCR alone and come to contradictory conclusions are at a methodological impasse (*14*, *15*). Moving to a simpler system to study bedaquiline action still requires an energy-transducing membrane, complicating experiments and providing more conflicting evidence. Inverted cytoplasmic membrane vesicles (IMVs) allow access to the active sites of respiratory enzymes whilst maintaining a proton-impermeable membrane, allowing the use of respiratory substrate oxidation assays and qualitative PMF reporters. However, IMVs provide inconsistent results with bedaquiline being found to uncouple succinate-energised IMVs (*15*), but not NADH-energised IMVs (*14*, *17*). (Proteo)liposomes have been used to show that at μM concentrations, bedaquiline can dissipate the PMF and that this activity is enhanced by the presence of *E. coli* ATP synthase (*16*).

By considering bioenergetic principles and reviewing the literature we formulate three hypotheses here for the mechanism of bedaquiline (also shown as a schematic in Fig1B-D). Activity 1- **uncoupler activity**: bedaquiline binding makes ATP synthase leaky to protons (*9*, *15*) or activates a proton carrier in the membrane (*14*) analogous to mammalian uncoupling proteins, in both cases having the functional effect of creating an uncoupler that collapses the PMF. Activity 2- **K^+/H^+**

ionophore activity: when bedaquiline binds to (tailgates) ATP synthase, a K^+/H^+ ionophore is created, which can selectively interchange ΔpH and transmembrane K^+ gradients (*16*). Activity 3-**oligomycin-like activit**y: bedaquiline binds to and jams ATP synthase like the canonical mammalian ATP synthase inhibitor oligomycin without additional effects; in this case how the cell responds creates the additional activities (*14*, *18*). We address these hypotheses by applying a new method to living mycobacteria: remission spectroscopy, which measures the visible-wavelength changes that occur as cytochromes (haem-containing bioenergetic complexes) donate or accept electrons as part of their function, measuring intracellular bioenergetic state (*19*). Critically, remission spectroscopy allows the use of turbid media so that measurements can be made on bacterial suspension cultures growing in defined conditions, offering a system for measuring mycobacterial bioenergetics and drug action within living cells. By combining remission spectroscopy with OCR measurements we break the methodological impasse to find that bedaquiline's dominant effect on cells is to act like oligomycin at both nM and μM concentrations; the previously reported increase in OCR stems from activation of the *bd* oxidase (Cyd). We show this activation occurs on the second time-scale, which is too fast for a transcriptional or translational change. A firm understanding of bedaquiline action *in vivo* provides a mechanistic basis for bedaquiline action and drug synergy, clarifies the importance of Cyd beyond O_2 scavenging in hypoxic conditions, and guides the development of future combination therapies against tuberculosis.

Results

A bioenergetic chamber allows simultaneous measurements of mycobacterial cytochrome redox state and oxygen consumption rate

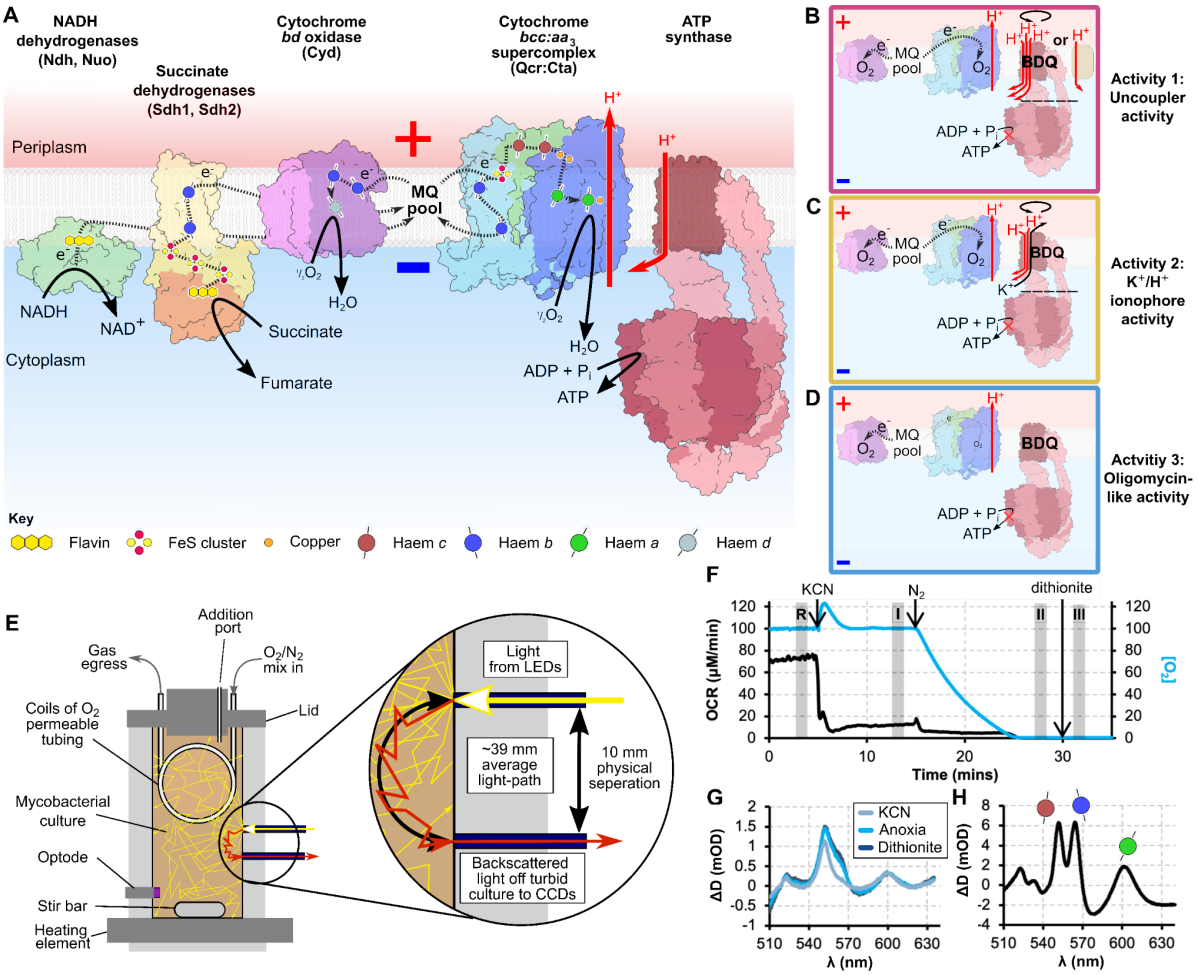

Figure 1. The bioenergetic chamber allows measurements of cytochrome spectra and oxygen consumption in living cells. (A) The mycobacterial oxidative phosphorylation system, including abundant cytochromes and ATP synthase. The cartoon is based on structural and functional information on NADH dehydrogenases (*20*), Sdh1 and Sdh2 (*21*, *22*), the *bd* oxidase (Cyd) (*23*, *24*), the respiratory supercomplex (*25–27*), and ATP synthase (*9*, *10*). Multimeric complexes are shown in their monomeric form. (B-D) The three activities tested in this work (E) The bioenergetic chamber, showing how the components interface with the bacterial culture (F) A representative experiment in the bioenergetic chamber. The chamber contained Msm (7H9 media + 50 mM glycerol) and the following changes were made: 1 mM KCN addition, having the gas-delivery tubing only contain N_2, and addition of sodium dithionite. $[O_2]$ in the culture and OCR are shown. The shaded periods are where spectra are averaged over. R is the reference period (G) Difference attenuance spectrum showing the reduction of cytochromes that occurs as KCN is added (spectrum I *minus* spectrum R), as the cells go anoxic (II *minus* R), and full reduction with dithionite (III *minus* R). (H) Difference spectrum of the purified respiratory supercomplex (cytochrome *bcc*:aa_3).

To establish that our system can make measurements on mycobacteria, we placed the model organism Mycobacterium smegmatis (Msm) in the chamber. OCR increased gradually as the cells grew (Fig 1F). The addition of KCN, a canonical inhibitor of aa_3-type oxidases, caused an increase in light attenuance and a drop in OCR, indicative of the oxidase being blocked and electrons

accumulating in the ETC. The increase in attenuance comes from the haem groups bound in the cytochromes, which are essential redox cofactors that change their absorbance depending on their redox state. KCN predominantly caused an increase in the electron occupancy of the *a* and *c* cytochromes (600 and 555 nm respectively), which have the highest E_m values, making them easy to reduce (Fig 1G). Removing O_2 further increased the electron occupancy of the *c*-cytochromes and induced a large increase in the *b*-cytochromes (565 nm); adding the strong reductant dithionite causes a final increase in *b*-cytochrome electron occupancy; at this point, the ETC was fully reduced.

Bedaquiline causes a redistribution of electrons in the mycobacterial ETC

We examined the effects of bedaquiline on Msm, where bedaquiline was first discovered (*6*). Msm was exposed to bedaquiline at nM concentrations and caused a small increase in OCR (Fig 2A), in line with previous observations (*14*, *16*). A marked increase in the electron occupancy of the *b* and *c* cytochromes (Fig 2D) was observed in the remission spectrum, indicating a back-up of electrons in the ETC that saturates at 30 nM. We compared bedaquiline to the ethanol vehicle and found that while ethanol caused a small increase in electron occupancy, bedaquiline caused a far greater increase (SF2).

To determine whether these changes required the binding of bedaquiline to ATP synthase, the bedaquiline-resistant $AtpE^{D32V}$ point mutant was explored (*6*). With the same concentrations of bedaquiline, the response was greatly diminished, with OCR only increasing in line with the growth of the cells in the chamber (Fig 2B). The remission spectrum changes are decreased and no longer saturate (Fig 2E and SF1), indicating that binding to ATP synthase is required for bedaquiline's effect on the ETC. Mtb exposed to bedaquiline behaved similarly (Fig. 2C and 2F), demonstrating the effect is conserved in the pathogen.

To unmix and quantify the individual cytochrome signals within the observed remission spectra, decomposition was applied (Fig 2G) (*28*). This approach separated the mixed spectra into individual cytochrome and background components (Fig 2I&J). Interestingly, while bedaquiline caused a robust increase in electron occupancy of the b_{557}, b_{565}, and *c* cytochromes, *a* changed little upon the addition of bedaquiline, despite the signal appearing clearly when cells are taken anoxic (Fig1G). While there is insufficient mechanistic information about the mycobacterial oxidase to explain this observation, mammalian systems respond similarly to oligomycin (*29*).

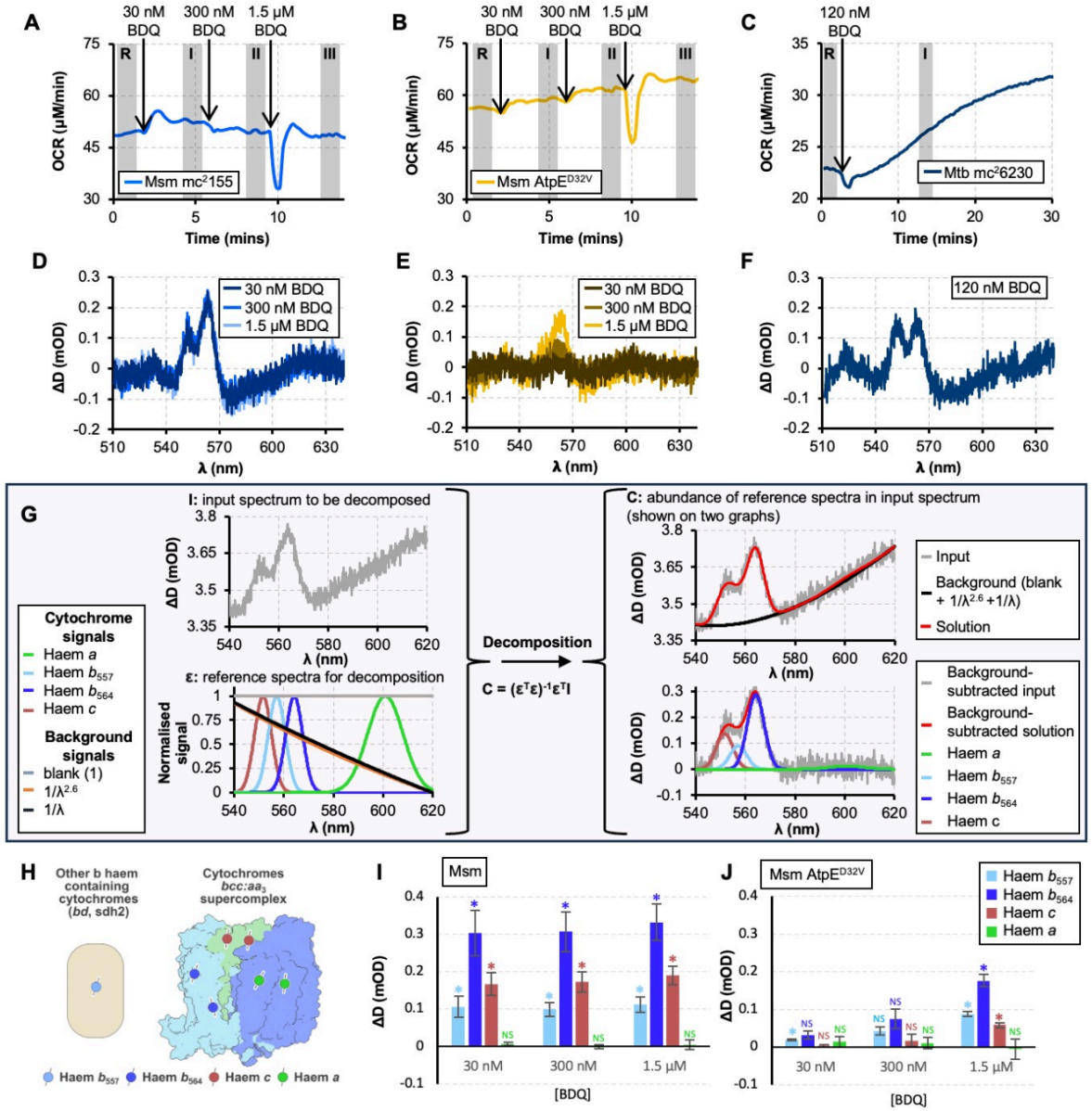

Figure 2. The effects of bedaquiline on Msm and Mtb measured in the bioenergetic chamber. (A, B, & C) OCR traces for Msm mc^{2}155, Msm AtpE^{D32V}, and Mtb mc^{2}6230 responding to the addition of bedaquiline (D, E, & F) Representative visible-wavelength difference remission spectra for the cultures in (A, B, & C); spectra were averaged over the shaded periods in (A, B, & C) and subtracted to give the presented spectra following a further subtract of a straight line. (G) Example of the spectral decomposition model and approach used here, showing the input spectrum and the reference spectra. On the right, the background components are shown on the input spectrum, demonstrating a reasonable fit. Below are input spectra with the background components subtracted, to clearly show the fit between model signals and the data. (H) Cartoon representation of the cytochrome complexes that correspond to the fitted signals (I & J) Results of fitting the signals on the runs above for both Msm mc^{2}155 and Msm AtpE^{D32V} providing individual cytochrome changes. Results representative of at least three independent experiments. * indicates a *p*-value less than 0.05, ** indicates a *p*-value less than 0.005, NS indicates an insignificant result; n = 3 in both I and J, panels A-F are representative replicates.

Resolving the mechanism of bedaquiline in living cells

Having established that the redistribution of electrons in the mycobacterial ETC responding to bedaquiline is measurable and quantifiable in our system, we set about systematically testing the mechanistic hypotheses in Fig1 through comparison with known bioenergetic effectors.

We first tested for uncoupling (activity 1) by examining the action of the established uncoupler CCCP. In Msm, low concentrations of CCCP cause an increase in OCR (Fig. 3A), consistent with an uncoupler that decreases PMF and stimulates respiration. In contrast to bedaquiline (Fig 2), CCCP caused the electron occupancy of b_{564} and *c* to decrease (Fig 3E&I). This decrease occurred because the *b*-cytochromes are buried in the membrane and are sensitive to ΔΨ (*30*). In Mtb, the change in b_{564} was not statistically significant but the electron occupancy of *c* significantly decreased; b_{557} (which is not part of the respiratory supercomplex) increased (Fig 3F&J). In both Msm and Mtb, higher concentrations of CCCP caused a collapse in OCR, with the cytochromes having even lower electron-occupancy, presumably due to the off-target effects of CCCP, demonstrating the importance of titrating CCCP. In sum, CCCP and bedaquiline both stimulate an increase in OCR but have opposite effects on the electron-occupancy of the supercomplex cytochromes b_{564} and *c*, inconsistent with bedaquiline having an uncoupling effect.

We next tested for K^+/H^+ exchange activity by examining the canonical K^+/H^+ ionophore nigericin. Interestingly, nigericin has different effects on Msm and Mtb. In Msm, there was a sudden drop in OCR and the electron occupancy of the *b* and *c* cytochromes decreased; after about 10 minutes, OCR recovered to near its starting point and the changes in the cytochromes began to revert (Fig 3C,G&K). In Mtb, OCR drops and fails to recover, accompanied by a large but variable increase in *c*, and a decrease in b_{564} electron occupancy. These observations show that nigericin acts differently in Msm and Mtb but in either case, does not match bedaquiline.

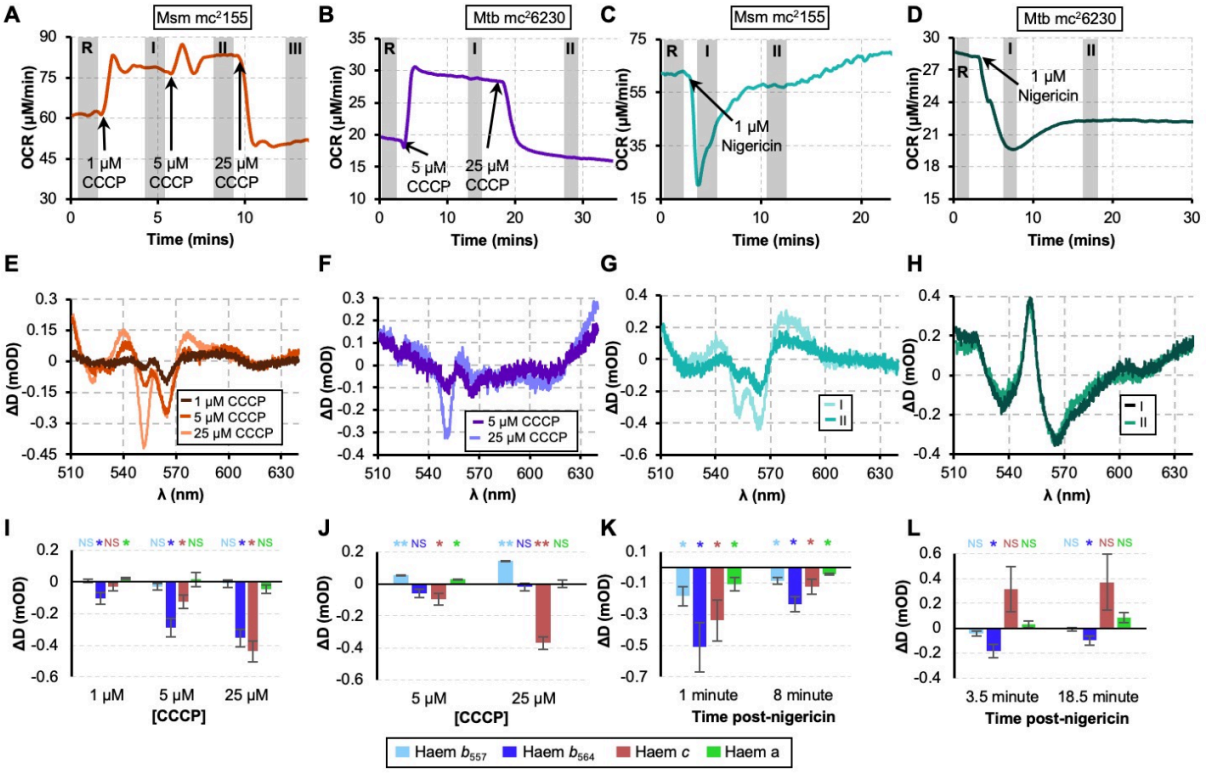

Figure 3. The effects of CCCP and nigericin on Mycobacterial OCR (A-D) and remission spectra (E-H). Data is presented for how CCCP affects Msm (A&E) and Mtb (B&F) and how nigericin affects Msm (C&G) and Mtb (D&H). (I-L) individual cytochrome changes resulting from quantification of the spectral changes for the panels above using the Gaussian unmixing model for three independent experiments. Cultures were concentrated to an OD_{600} of ~1.8 (Msm) and ~5 (Mtb) for analyses. The oxygen concentration in the chamber was held at 100 µM. Cells were suspended in 7H9 + 50 mM glycerol; 0.2 mM pantothenate was added in experiments with Mtb. * indicates a *p*-value better than 0.05, ** indicates a *p*-value less than 0.005, NS indicates an insignificant result; n = 3 in I, J, K, and L.

To corroborate these findings, we examined the effect of the covalent ATP synthase inhibitor DCCD on Msm. DCCD behaved similarly to bedaquiline: inducing a small increase in OCR and an increase in the electron occupancy of the *b*- and *c*-cytochromes (SF3A-C). To measure DCCD and BDQ's effects on ΔΨ and ΔpH we used an isotope accumulation assay on whole cells (*15*). Treatment with bedaquiline or DCCD significantly increased ΔΨ relative to a DMSO control, while neither had a significant effect on ΔpH (Fig SF3D,E), consistent with bedaquiline acting as an oligomycin-like inhibitor.

The *bd* oxidase (Cyd) acts as a 'relief valve' to protect cells from bedaquiline action

Bedaquiline's lack of protonophoric or ionophoric activity left us with activity 3: oligomycin-like activity. To accept this activity, there needs to be a mechanism to explain the remarkable increase in OCR that bedaquiline induces. One possibility is that in response to bedaquiline, flux is rerouted from the supercomplex to the *bd* oxidase, Cyd. Cyd does not pump protons, its activity only builds the PMF by releasing protons into the periplasm as it oxidises MKH_2. It is therefore much less sensitive to the PMF than the supercomplex and could act as a 'relief valve' for electron flux when the PMF is high. To test this hypothesis, we moved to strains with deletions of the *cydAB* operon in Mtb (*31*) and Msm (*32*). We attempted to use the characteristic *d* cytochrome signal to detect changes to Cyd at 630 and 650 nm (*23*, *24*, *33*) using a wide spectrum but the changes were too small compared to noise to be reliably interpreted (SF5 A&B). However, spectra of isolated cytoplasmic membranes showed clear levels of Cyd in Msm grown aerobically at pH 6.6 (SF 4E), which was reduced in Δ*cydAB* (SF5 E,F). There is a second *bd* oxidase (AppCB) present in Msm but not Mtb (*34*), which may explain the small *d* cytochrome present in Msm Δ*cydAB*.

When Msm Δ*cydAB* was exposed to 30 nM bedaquiline there was an immediate decrease in OCR, while the electron occupancy of *b* and *c* cytochromes increased as before (Fig 4A&E). This is consistent with the behaviour of oligomycin in mitochondria, demonstrating that Cyd mediates the increase in OCR in response to bedaquiline. However, this effect is less pronounced in Mtb Δ*cydAB*: OCR increases, but at a slower rate (Fig 4B). We speculated this was due to one of two reasons: (1) bedaquiline is less capable of reaching its target site in Mtb through differences in bedaquiline influx or efflux or (2) Mtb's bioenergetic system has additional mechanisms to compensate for the backpressure induced by bedaquiline. If the differences were due to the ability of bedaquiline to reach its target site, increasing the concentration of bedaquiline should overcome it. When the concentration of bedaquiline was increased to 10 μM, there was a robust decrease in OCR in both Msm and Mtb Δ*cydAB* (Fig 4C,D). The differences observed may have been due to the differences in expression of the MmpS5-MmpL5 transporter, which is implicated in bedaquiline efflux (*35*).

Taking bedaquiline from nM to μM concentrations also tests the hypothesis that only at μM concentrations does bedaquiline act as an uncoupler, either as a small molecule proton transporter or at ATP synthase (*9*, *16*). The remission spectra of an uncoupler would have been expected to resemble that of CCCP as bedaquiline concentration was increased to 10 μM, indicating a decrease in electron occupancy. Instead, no significant change in Msm or Mtb (Fig 4 and SF4) was observed, demonstrating that bedaquiline does not act as an uncoupler at higher concentrations.

Our results have shown that the canonical relationship between ATP synthase activity and OCR is not as reliable as previously thought. While prior studies found that the addition of bedaquiline leaves OCR in mammalian cells unchanged (*14*, *36*), recent work found that bedaquiline inhibits the *in vitro* activity of human mitoplasts and purified ATP synthase with an IC_{50} of ~ 500 nM (*10*, *11*), below concentrations found in patient sera (1.8-8.9 μM) (*37*). To determine whether bedaquiline was capable of inhibiting human mitochondrial function, the effects of bedaquiline on a

human cell line were tested (HEK293T). When bedaquiline was added at 10 μM, no difference in the remission spectrum or OCR compared to ethanol (the vehicle) or nothing was observed; in contrast, the canonical inhibitor oligomycin A caused an increase in both *b* and *c*-cytochrome electron occupancy (Fig4O-Q, Fig SF6). Combined with the observations that bedaquiline is found in mitochondria at low concentrations compared to other parts of the cell (*38*) we conclude that bedaquiline simply does not reach mammalian ATP synthase at sufficient concentration to cause inhibition.

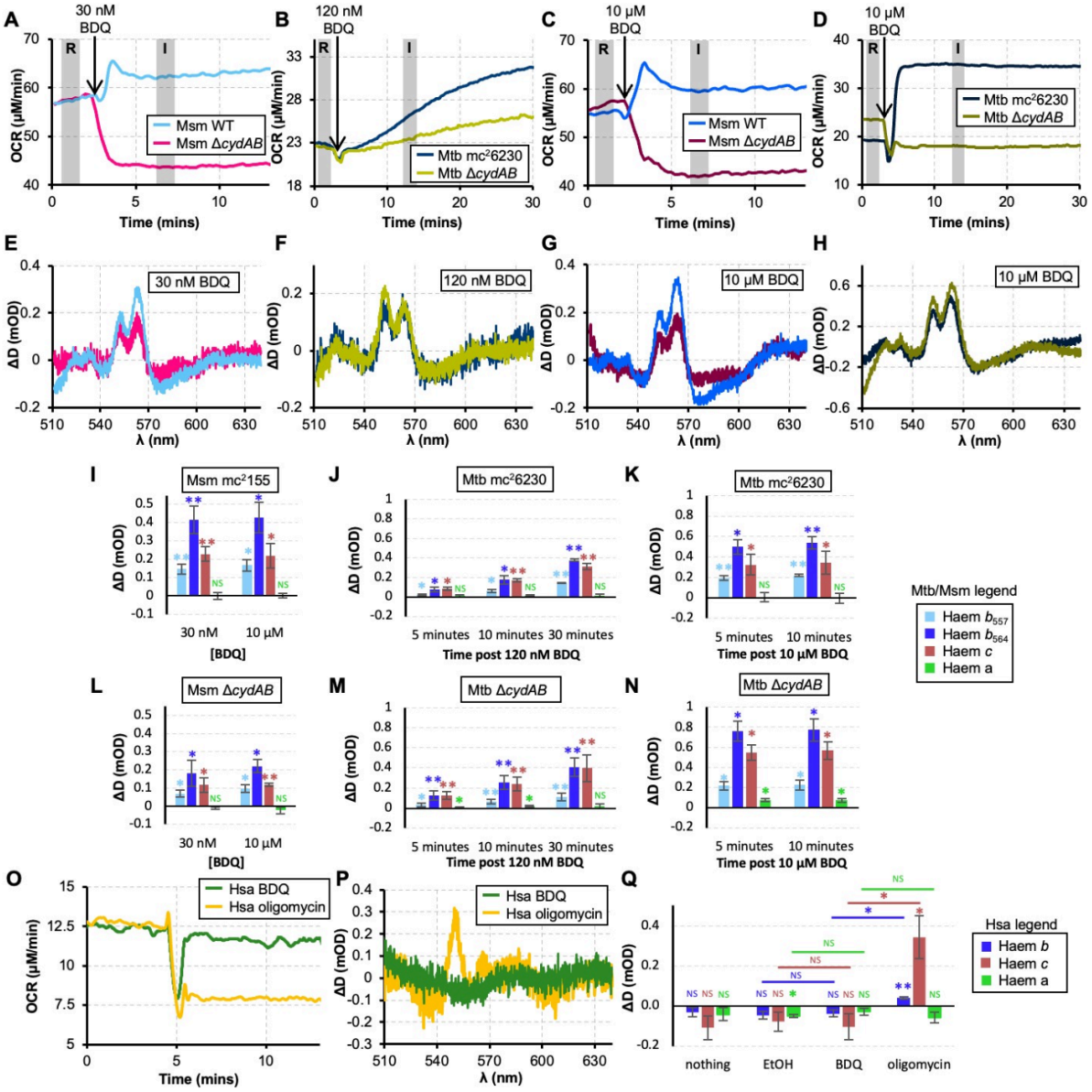

Figure 4. The effects of nanomolar and micromolar concentrations of bedaquiline on Msm, Mtb, and human cells (Hsa). (A-D) OCR of Msm mc^{2}155 and Δ*cydAB* and Mtb mc^{2}6230 and Δ*cydAB* responding to nM and µM concentrations of bedaquiline. (E-H) Remission difference spectra for the same cultures as in (A-D). (I-N) Changes in individual cytochromes for Msm mc^{2}155 and Δ*cydAB* and Mtb mc^{2}6230 and Δ*cydAB* on the addition of bedaquiline. (O-Q) Changes in OCR, remission spectra, and individual cytochromes for human HEK293T cells exposed to 10 µM bedaquiline or 1.5 µM oligomycin. B and F include data from Fig 2C&F for comparison. Values for changes in attenuance and OCR were recorded 3 minutes post-addition for Msm, 10 for Mtb, and 5 for Hsa. The oxygen concentration in the chamber was held at 100 µM. Cells were suspended in 7H9 + 50 mM glycerol 50 mM; 0.2 mM pantothenate was added in experiments with Mtb. For individual cytochrome signals in panels (I-N, & Q) * indicates a *p*-value < 0.05, ** indicates a *p*-value < 0.005, NS indicates an insignificant result; n = 3 for all except Msm mc^{2}155 responding to 30 nM bedaquiline and Mtb Δ*cydAB* responding to 120 nM bedaquiline, where n = 5. For the pairwise comparisons in (Q), * indicates a *p*-value < 0.025, to account for multiple comparisons.

Discussion

Of the three possible hypotheses set out in Fig1, our results are inconsistent with bedaquiline acting as an uncoupler or ionophore (activities 1 and 2). Our model for action is as follows: bedaquiline binds to the ATP synthase c-ring, stopping catalysis. As catalysis is stopped, the major conduit of H^+ from the periplasm to the cytoplasm is blocked, increasing PMF (backpressure) that resists forward-catalysis by the ETC. As the respiratory supercomplex is strongly PMF-coupled, its catalysis is slowed, decreasing OCR. However, Cyd is rapidly activated, allowing OCR to increase beyond pre-bedaquiline levels.

Previously, the nature of backpressure within mycobacterial bioenergetics had been questioned, with proposals that it is either not sensed or collapsed by adaptive mechanisms (*14*). By directly measuring the status of the ETC in vivo, we find that bedaquiline increases backpressure and the ETC directly senses it. Our Δ*cydAB* experiments in both Mtb and Msm show that any induction of an adaptive response beyond redirection of flux must either be absent or have a minimal effect on PMF. This backpressure explains why bedaquiline induces increased succinate accumulation and elevated $NADH/NAD^+$ levels (*12–14*), signatures of backpressure in mammalian systems (*38*, *39*).

The *bd* oxidases such as Cyd are traditionally seen as O_2 scavenging enzymes (*33*). However, their affinity for O_2 does not explain their role in pathogenesis: the apparent K_M of the mycobacterial respiratory supercomplex for O_2 is ~0.9 μM (*40*), and mediates growth at oxygen concentrations below the ~2 μM O_2 within granulomas (*41*). Cyd compensates for loss of the supercomplex during infection (*42*), but its specific function within the branched mycobacterial respiratory chain is unclear. Here, we find a role for Cyd as a relief valve for reductive pressure at plentiful O_2. This also explains Cyd's function in acid tolerance, where Mtb experiences reductive pressure (*43*, *44*).

Our results provide insights into bedaquiline tolerance and antimicrobial synergy. First, Cyd's capacity to relieve bedaquiline-induced backpressure provides a mechanism for its role in bedaquiline tolerance (*15*, *18*). Second, the shift in flux from the supercomplex to Cyd explains the lack of synergy between supercomplex inhibitors and bedaquiline (*45*) or its analogues (*46*). A Cyd inhibitor could mitigate these challenges as demonstrated by their enhancement of the bactericidal activity of bedaquiline and supercomplex inhibitors (*31*, *47*). Finally, we can explain the synergy between clofazimine and bedaquiline (*14*, *48*). Clofazimine is reduced by NDH-2, whereupon it redox cycles, creating ROS (*49*). As measured in our remission spectra, backpressure causes the electron occupancy of the ETC to increase. This backpressure-induced reduction will in turn reduce NDH-2, increasing its side-reaction with clofazimine and generation of ROS.

Previous work relied on combining OCR measurements on intact bacilli with measurements on inverted membrane vesicles (*14–16*). The advantage of our approach is that a single bacterial culture provides sufficient information to discern the mechanism of the added bioenergetic-effector, avoiding effects arising from differences between intact cells, IMVs, and (proteo)liposomes. IMVs have long been a bioenergetic experimental system but only partially resemble cells. Whilst they sustain a PMF across their membrane, the polarity of the inner phase is reversed (i.e. the negative and alkali cytoplasm/matrix becomes the positive and acidic IMV/SMP lumen) and the membrane area-to-volume ratio differs by orders of magnitude (~100 μm^2 fL^{-1} in IMVs vs ~0.2 μm^2 fL^{-1} in bacteria) (SF7). Protonophoric agents require both the charge-driven movement of the ionic form and the neutral diffusion of uncharged form across the membrane to occur at a reasonable rate but the balance of which is limiting is highly dependent on the system and state (*50*). As such, the chemical differences between bedaquiline and FCCP/CCCP may explain why bedaquiline uncouples IMVs and not intact cells: Bedaquiline has a pKa of 8.9, with neutral and positively charged forms while FCCP

and CCCP have pKa's of 6.2 and 5.6 respectively with neutral and negative forms. FCCP/CCCP will effectively uncouple intact bacteria but is a relatively poor uncoupler of IMVs; e.g. fully uncoupling mammalian IMVs requires the use of gramicidin (*51*). As bedaquiline's charge states are reversed, most likely it uncouples IMVs but not intact cells.

The study of bioenergetics has historically relied on combining quantitative measurements made on purified or minimal systems and cruder measurements made on intact cells. Our approach allows quantitative measurements to be made in living mycobacteria and offers a clear mechanism for bedaquiline and insights into mycobacterial physiology. Cytochromes are near-universal in O_2-consuming organisms, allowing this approach to be applied broadly in the future.

Supplementary figures

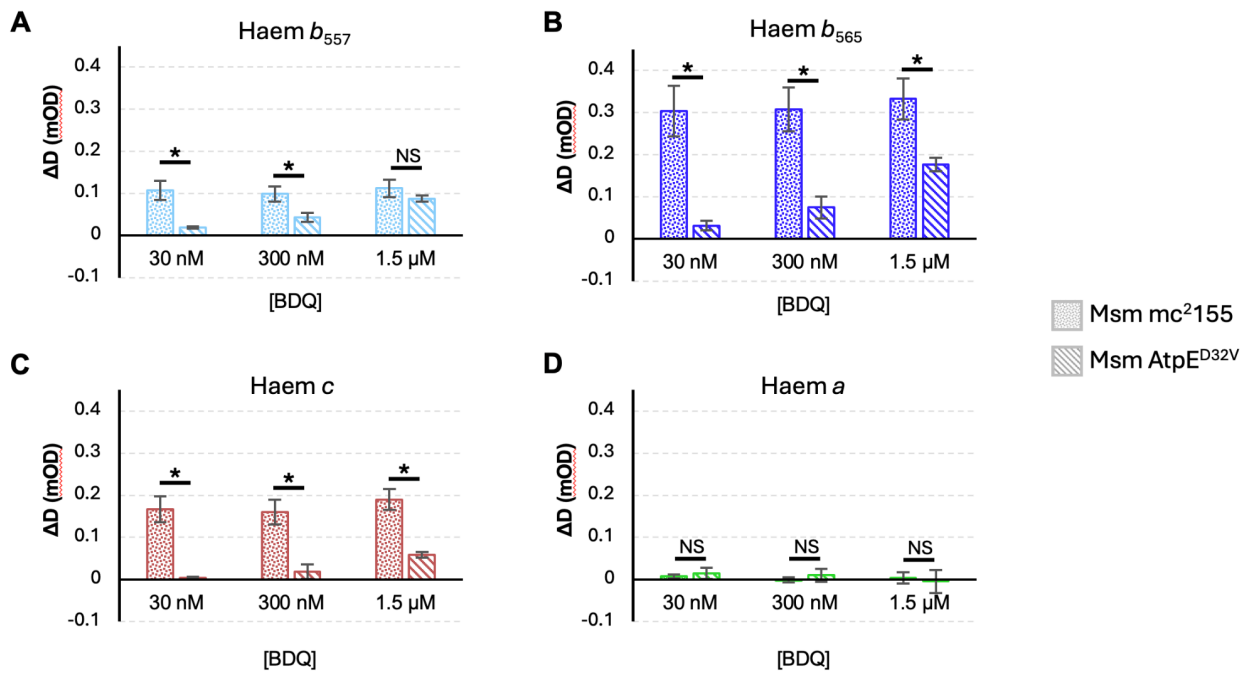

SF1. Comparison and statistical analysis of cytochrome signals in Fig. 2. Data from three independent experiments. * indicates *p*-value < 0.05, NS indicates an insignificant comparison.

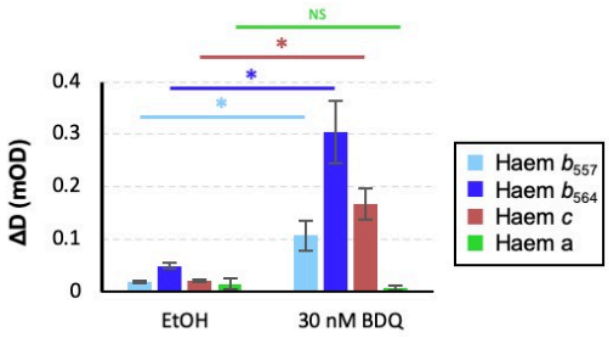

SF2. Comparison of ethanol addition alone and bedaquiline dissolved in ethanol in Msm. The bedaquiline response is significantly higher than EtOH vehicle alone; 5 µL of EtOH was added to the 5mL chamber. * indicates p-value < 0.05, NS indicates an insignificant comparison.

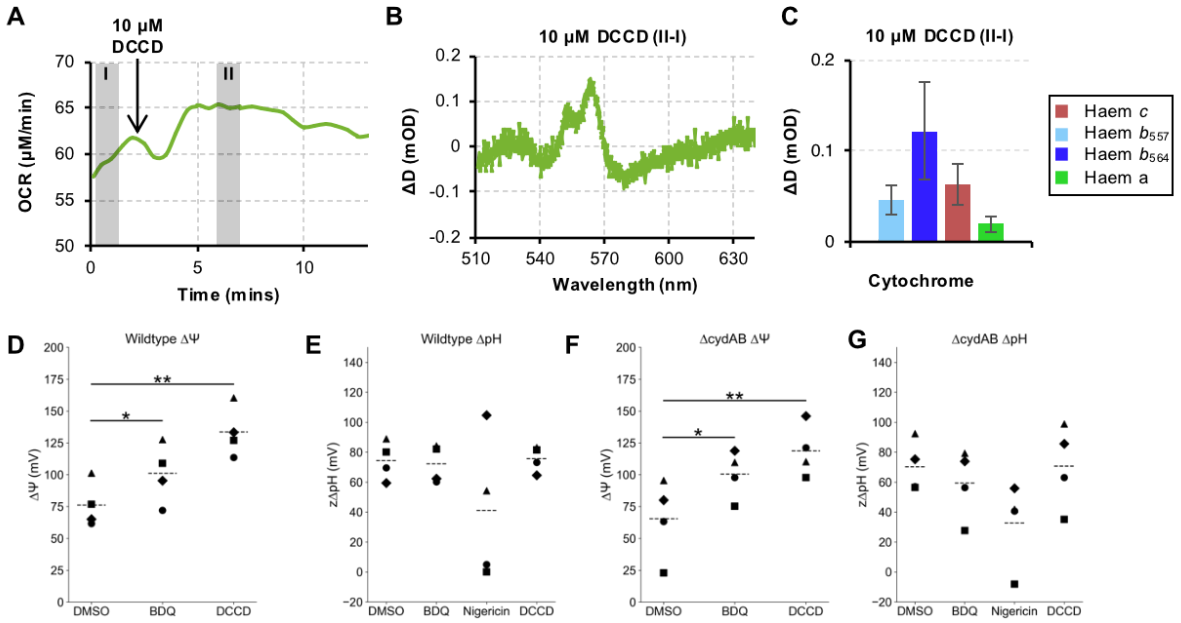

SF3. Effect of DCCD on Msm and PMF measurements of Msm in response to bedaquiline and DCCD (A-C) OCR traces, remission spectra and changes in individual cytochromes of Msm in response to DCCD, n=3 independent experiments. (D-G) Effect of bedaquiline and DCCD on bioenergetic parameters measured with [^{3}H]TPP^{+} (ΔΨ) and [7-^{14}C]benzoate (ΔpH). (D) ΔΨ of Msm after treatment with DMSO, bedaquiline, and DCCD (E) ΔpH of Msm after treatment with DMSO, bedaquiline, nigericin, or DCCD (F) ΔΨ of Msm Δ*cydAB* after treatment with DMSO, bedaquiline, and DCCD (G) ΔpH of Msm Δ*cydAB* after treatment with DMSO, bedaquiline, nigericin, and DCCD. Symbols represent matched replicates from n=4 biological replicates, dashed lines indicate mean. * indicates *p*-value < 0.05, ***p*-value < 0.01. Repeated Measures ANOVA with Bonferroni correction.

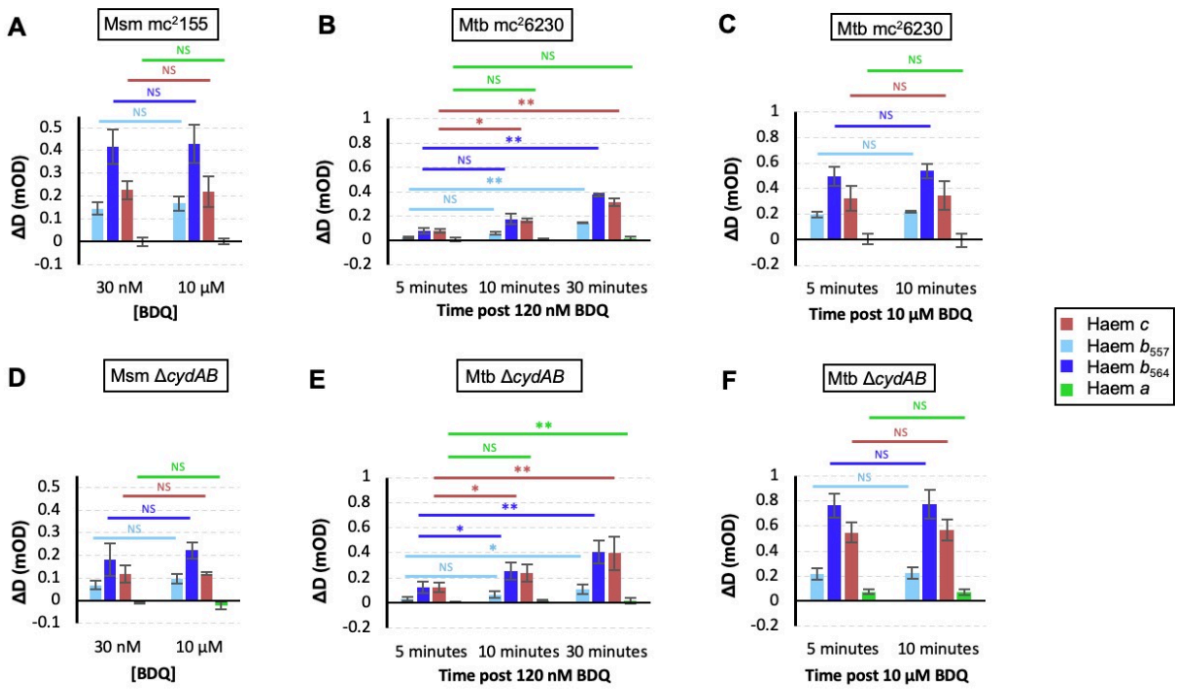

SF4 - Statistical comparisons between datasets in Figure 4. All tests are 2-tailed T-tests between groups with unequal variance. For (A, C, D, and F) no significant difference was found for pairwise comparisons. For (B) and (F), * indicates a *p*-value better than 0.025, ** indicates a *p*-value better than 0.0025 to account for the multiple comparisons.

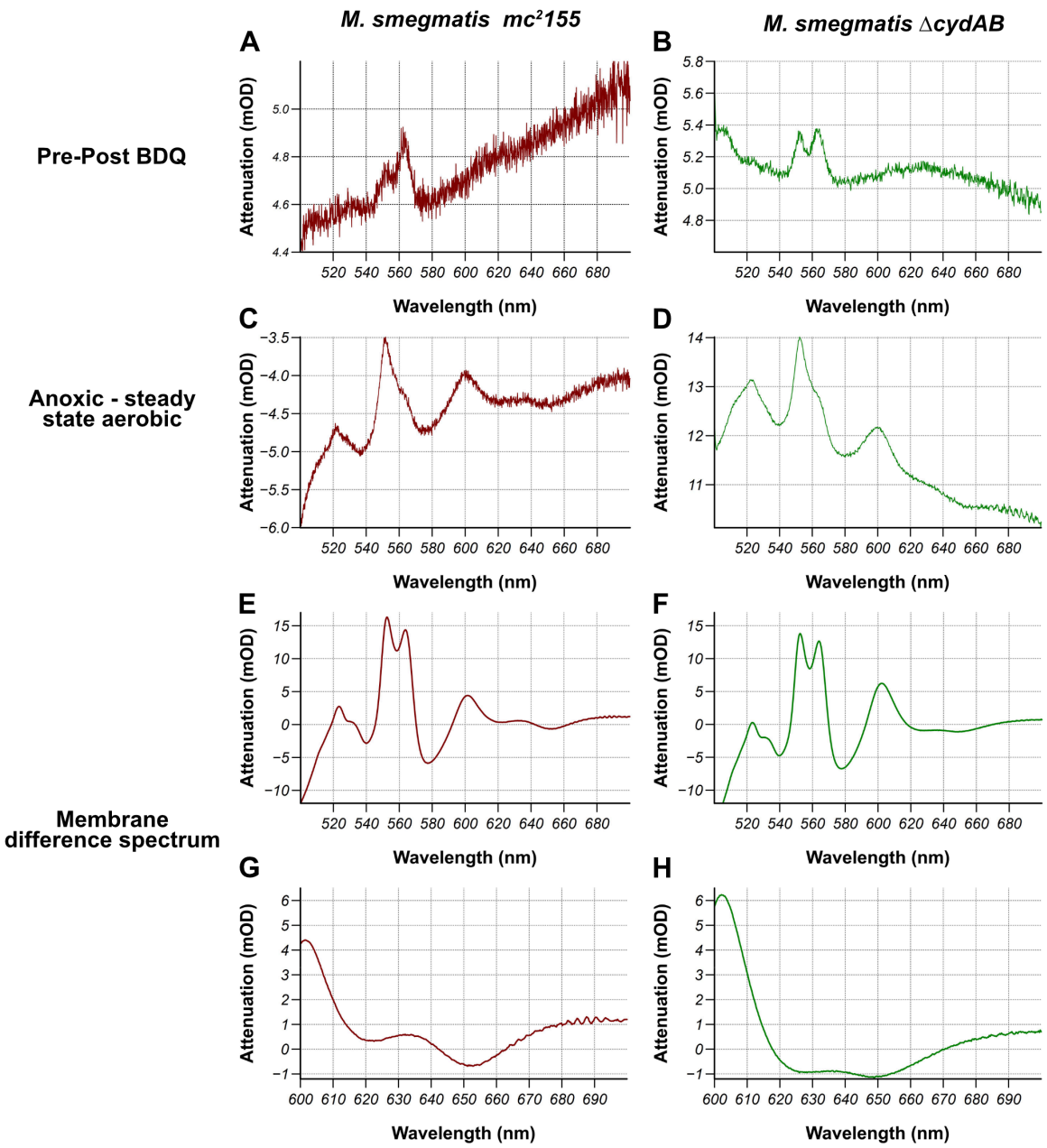

SF5- Wide-spectra of cells and isolated membranes to detect redox changes in Cyd in WT Msm and Δ*cydAB* Msm (A & B) The spectral response to the addition of 30 nM bedaquiline in mc^{2}155 Msm (maroon) and Δ*cydAB* Msm (green). Any difference in the region around the cytochrome *a* and cytochrome *d* signals are not above the noise of the spectrum. (C & D) Anoxic spectrum minus the aerobic steady state spectrum from mc^{2}155 Msm and Δ*cydAB* Msm, intact cells. (E & F) Reduced-oxidised spectra of mc^{2}155 Msm membranes (E) and Δ*cydAB* Msm membranes. (G & H) Comparison of the cytochrome *d* spectral region of mc^{2}155 and Δ*cydAB*.

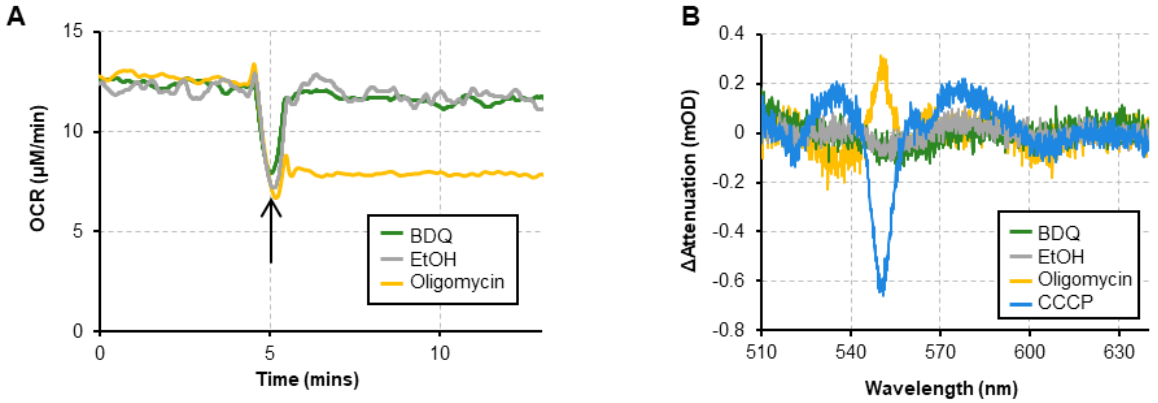

SF6- Effect of bedaquiline and respiratory inhibitors on the human HEK293T cell line. (A) OCR traces of HEK293T cells treated with 10 µM bedaquiline (BDQ), ethanol vehicle control (EtOH), and 1.5 µM oligomycin A. Arrow indicates the time point at which drug was added. (B) Difference spectra of HEK293T cells treated with 10 µM bedaquiline, ethanol, 1.5 µM oligomycin A, and 1 µM CCCP. Data are representative of n=3 independent experiments.

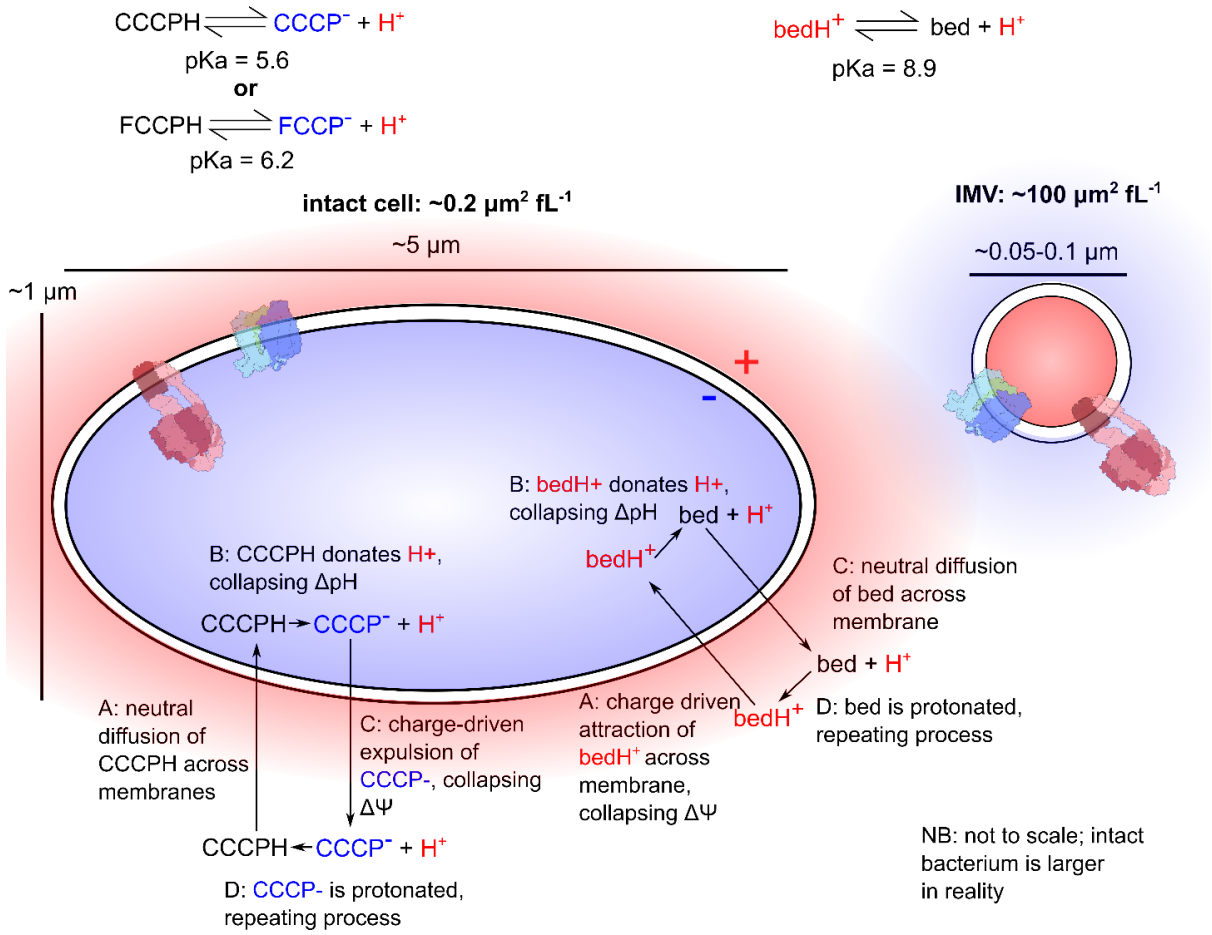

SF7- Schematic of differences between intact bacteria and IMVs and how this may affect uncoupling by different agents. The polarity of the structures is reversed, with negative/alkali conditions being found inside intact cells and positive/acid conditions being found in the lumen of IMVs. Additionally, the surface area to volume ratio is different; here the ratio was calculated assuming IMVs are spherical and bacteria are cylinders with hemisphere ends. Chemical uncouplers like FCCP and CCCP have neutral protonated forms and negative deprotonated forms, whereas bedaquiline has a positive protonated form and a neutral deprotonated form. These differences may explain why bedaquiline can uncouple IMVs but not intact cells.

Materials and Methods

Materials and Strains

Bedaquiline, CCCP, nigericin, DCCD, and oligomycin A were purchased from AdooQ Bioscience, Alfa Aesar, Cayman Chemical Company, Sigma-Aldrich, and MedChemExpress, respectively. For chamber experiments these compounds were dissolved in EtOH and for isotope accumulation assays were dissolved in DMSO.

Msm strains used are mc^2155 WT, $AtpE^{D32V}$ and Δ*cydAB*. $AtpE^{D32V}$ is mc^2155 with a point mutation in the *atpE* gene conferring bedaquiline resistance (*6*) and Δ*cydAB* is mc^2155 with deletion of the *cydAB* gene (*32*). Mtb strains used were H37Rv ΔRD1 Δ*panCD* (mc^26230) (*52*) the Δ*cydAB* strain used in this study is Mtb mc^26230 with a deletion of the Δ*cydAB* locus(*31*).

Growth Conditions

Msm strains (mc^2155, Δ*cydAB* and $AtpE^{D32V}$) were grown in Middlebrook 7H9 media (Sigma-Aldrich) supplemented with Tween 80 (0.05 % v/v) and glycerol (50 mM). For the $AtpE^{D32V}$ strain, 5mM D-(-)-arabinose was added to reduce clumping. Media and supplements, save for D-(-)-arabinose, were combined prior to autoclaving. 7H10 agar plates supplemented with glycerol (68 mM) were inoculated with a -70°C glycerol stock and incubated at 37°C for ca. 72 hours. Once single colonies were visible, plates were stored at 4°C and single colonies were used to inoculate 50 mL of media in 250 mL conical flasks to prepare starter cultures. These cultures were incubated (37°C, 200 rpm) until an OD_{600} of 2.5-5 was reached (ca. 72 hours).

Mtb strains (mc^26230 and Δ*cydAB*) were grown in Middlebrook 7H9 media (Sigma-Aldrich) supplemented with Tween 80 (0.05 % v/v), glycerol (55 mM), Middlebrook OADC growth supplement (bovine albumin fraction V (50 g/L), D-glucose (20 g/L), catalase (0.04 g/L), oleic acid (0.5 g/L), sodium chloride (8.5 g/L)) (10 % v/v) and pantothenate (48 mg/L). Tween 80 and glycerol were added prior to autoclaving with other supplements being added after. 5 mL of media in 25 mL vented flasks were inoculated from a -70°C glycerol stock and incubated at 37°C for 3-4 weeks.

HEK293T cells (ATCC CRL-3216) were cultured at 37ºC in phenol-red free DMEM (Gibco) supplemented with 10% v/v foetal bovine serum (Gibco) in a 5% CO2 incubator.

Preparing cells for measurements in the bioenergetic chamber

Initial experiments indicated that washing cells without detergent lowered the concentration at which the effect of metabolic effectors could be observed in the system, presumably due to partitioning of lipophilic compounds into the detergent. 50 mL Msm cultures were grown to mid-exponential phase in an orbital shaking incubator in 250 mL conical flasks. 3-5 mL of culture was pelleted in a swinging-bucket centrifuge at 3894xRCF for 5 mins at 37°C. Cells were then washed and resuspended in 5mL medium to an OD_{600} ~1.5. Mtb was grown in 40 mL cultures in vented T175 flasks to an OD_{600} between 0.7-1.0. 35 mL of culture was pelleted in a swinging-bucket centrifuge at 3894xRCF for 5 mins at 37°C. Cells were then washed and resuspended in 5mL of medium without detergent or OADC to an OD_{600} of ~6. Given the approximate OD values above, the normalised OCR was ~40 µM/min/OD for Msm and ~3 µM/min/OD for Mtb.

HEK293T cells were grown in T175 flasks to ~70-80% confluency. Cells were harvested by treatment with 0.05% Trypsin-EDTA (Gibco). Harvested cells were pelleted for 3 minutes at 500xRCF and resuspended to a final concentration of 1.0 x 10^7 cells/mL in FluoroBrite DMEM (Gibco),

supplemented with 4 mM L-Glutamine and 25 mM HEPES pH 7.4. 5 mL of this suspension was used for chamber measurements.

Bioenergetic Chamber Measurements

Measurements were made using a prototype of the Iberius Cell Spectroscopy System (CellSpex Ltd); many components were transferred from a system previously used to make measurements on mammalian cells (*19*, *39*). The bioenergetic chamber is composed of three systems integrated together: a culture vessel, a remission spectroscopy system, and an oxygenation system. These are described in turn but work together simultaneously.

The culture vessel is composed of a 5 mL quartz crucible set into an aluminium block. Optodes for [O_2] measurement and remission spectroscopy are inserted through the crucible to access the bacterial culture. A magnetically-driven glass-covered stir bar run at 700 rpm is used to mix the culture and the system is maintained at 37°C thermoelectrically.

For remission spectroscopy, a warm white light emitting diode (Luxeon-CZ 4000K-90 run at 300mA) was used to illuminate the culture through a 2.0mm NA0.5 POF optical fibre. Reemitted light back-scattered from the culture was collected with a 1.0mm NA0.37 silica fibre located 10 mm below the illumination fibre. Previously the pathlength of such a setup has been measured as ~39 mm, using the 2nd deferential techniques of the 740 nm absorption band of water (*29*). The collected light was fed into a Triax 320 spectrographs (Horiba) equipped with a DV401BV back-thinned charged coupled device (CCD; Andor Technology). Each spectrum was collected for 6 ms and 50 were averaged together every 0.5 s to give each working spectrum. For narrow spectra, the spectrograph was set to detect over the wavelength ranges 509- 640 nm, with a 600 groove / mm grating blazed at 500 nm and slit widths set to 200 microns. For the wide spectra, the spectrograph was set to detect over the wavelength ranges 481 - 751 nm, with a 300 grooves / mm at blazed 500 nm and slit widths set to 100 microns. For wide spectra, it was necessary to subtract the contribution from the optode phosphorescence at 650 nm, so the CCD collected 2 phases, phase one where the LED was on, and phase 2 where the LED was off. The output spectrum was then phase 1 minus phase 2. The spectrograph was calibrated daily against mercury emission lines (546.074 nm, 576.960 nm, and 579.070 nm). The spectra resolution in both cases was ≈1nm.

The oxygenation system relies on measuring dissolved O_2 and delivering oxygen, via gas-permeable silicone tubing (Renasil©, Braintree Scientific) immersed in the suspension, at a rate equal to the rate consumed by the cells such that the oxygen concentration is constant. The oxygen consumption was then calculated from the rate of oxygen delivery corrected for the rate of change of oxygen concentration in the chamber. The rate of oxygen delivery was controlled by changing the N_2/O_2 gas mixture flowing through the tubing using a gas blender, and a feedback circuit varied the gas mixture to maintain the dissolved oxygen concentration at a set value. Oxygen tension was measured from the phase shift from a phosphorescent membrane (oxygen optode) using a phase fluorimeter (CellSpex Ltd). When compounds were added from cold ethanolic stocks, there was typically a spike in OCR, occurring because of the O_2 dissolved in the stock solution, before a new steady state is set. When OCR changes rapidly, often the spike is obscured. In either case, rates were measured only after the spike had settled. The optode was calibrated every few weeks to ensure accuracy and the permeability of the tubing was calibrated before every experiment.

Spectral and statistical analysis

In a remission geometry, attenuance (D) is defined as:

$$D = -log_{10}\left(\frac{I}{I_0}\right)$$

Where I is the detected light intensity as a function of wavelength and I_0 is the illumination light intensity as a function of wavelength.

The changes to spectral attenuance induced by inhibitors or other changes were measured as deflections (difference spectra) from a reference period. The average attenuance (D) over the reference period was subtracted from the period of interest to give ΔD spectra. Typically, the periods were 0.5-2 minutes long to give sufficient signal for interpretation. For the display of ΔD spectra, a straight line is subtracted to account for changes to the baseline.

For unmixing, cytochrome and background signals from the observed mixture in the ΔD remission spectrum we used decomposition with model cytochrome signals composed of Gaussian functions. The observed *b*, and *c* peaks are each composed of at least 6 and 2 individual cytochromes respectively, changing independently of each other ($c = c_1$ and c_2 in the respiratory supercomplex, *b* = two *b* cytochromes in the Qcr component of the respiratory supercomplex, two in Cyd, and two in Sdh2). Signals for cytochrome *c*, cytochrome b_{564} and cytochrome *a* were included based on the spectrum of the purified supercomplex. To account for the other *b*-cytochromes, a signal centred at 557 nm was included and gave a solution that accounted for nearly all of the observed signal, judged by the flat residual spectrum.

To determine the magnitude of spectral signals, the difference spectra were fitted using a linear combination of Gaussian peaks and background functions (1 , $1/\lambda^{2.6}$, $1/\lambda$). This was performed with decomposition using Eq. 1

$$C = \left(\varepsilon^T \varepsilon\right)^{-1} \varepsilon^T \Delta D \qquad [1]$$

where **C** is a column matrix containing the contribution of each of the components. **ΔD** is a column matrix containing the attenuance difference at each wavelength and **ε** is a matrix containing each of the gaussian or background components.

Each of the cytochrome functions is described by Eq. 2:

$$y = e^{-Ln(2)\left(\frac{\lambda-\lambda_0}{w/2}\right)^2} \qquad [2]$$

Where *c* is the centre of the peak and *w* is the full width at half maximum. For *M. smegmatis* and *M. tuberculosis*, the values for *c* and *w* for each peak is as follows, cytochrome *c* (551.5, 8), cytochrome b_{557} (557.0, 8), cytochrome b_{564} (564.0, 8) and cytochrome *a* (600.7, 17). For *H. sapiens*, the values were cytochrome *c* (550.5, 8.5) cytochrome *b* (564.0, 9) and cytochrome *a* (600.7, 17). All the components, peaks and background functions, were normalised across the fitted wavelength range such that the maximum was 1 and the minimum was 0.

To estimate when the system is detecting and fitting an individual cytochrome signal above noise we use a one-sample T-test (*53*). The ΔD spectrum of the reference period is 0 so the null hypothesis (H_0) is that there is no difference in the data from 0 and the alternative hypothesis (H_A) is that there is.

$$t = \frac{\bar{Y} - \mu_0}{SE_{\bar{Y}}} \qquad [3]$$

Where t is the t-statistic, $\bar{Y}$ is the mean, μ_0 is the mean proposed by H_0, in this case 0, and $SE_{\bar{Y}}$ is the standard error.

For comparisons between conditions a 2-tailed T-test was used, assuming unequal variance (Welch's T-test). When needed, Bonferroni correction for multiple comparisons was applied to the p-values needed to ascribe significance to results.

Isolation of the 3xFLAG QcrB respiratory supercomplex (cytochrome *bcc:aa*$_3$)

As in (*54*) an Msm strain with a 3xFLAG tag at the C-terminus of the *qcrB* subunit of the supercomplex was generated with the ORBIT method (*55*). The Msm strain was cultures as before except the starter culture was used to inoculate 1 L cultures in 2.5 L baffled flask (200 rpm 37°C). These were grown until an OD_{600} of 0.8 was reached at which point they were harvested via centrifugation (5000 *g*, 20 mins, 4°C, SLC-6000 rotor). The cells were then homogenised in ~5 mL of chilled lysis buffer (50 mM Tris-SO4 pH 7.4 (RT), 150 mM NaCl, 5 mM EDTA, 1 mM $MgCl_2$) per g of cell weight and frozen until required.

After thawing and the addition of protease inhibitor tablets (Roche) (1 per 50 mL) and DNase (1 mg/mL), the cells were broken with 3 passages at 40 kpsi through a cell disruptor (Constant Systems). Unbroken cells and debris were pelleted by centrifugation (48 kx*g*, 12 mins, spin, 4°C, SS-34 rotor), followed by a longer ultracentrifugation spin to pellet the membranes (150 k*g*, 2 hrs, 4°C, Type 45Ti rotor). These membranes were washed by resuspending and pelleted via an identical spin. The washed membranes were then resuspended at ~10 mg/mL to then be stored at -70°C.

To isolate the 3xFLAG QcrB *bcc:aa*$_3$, membranes were thawed and diluted to 5 mg/mL, as determined by a BCA assay, using the purification buffer (50 mM Tris-SO4 pH 7.4 (RT), 150 mM NaCl). They were then incubated with 1 % DDM for 40 mins at 4°C with agitation. Unsolublised material was then removed via ultracentrifugation (150 kx*g*, 30 mins, Type 70.1 Ti rotor, 4°C). The Anti-FLAG® M2-affinity gel (Merck) was washed twice and then resuspended in the binding buffer (purification buffer, 0.02% DDM). This was then added to the solubilised membrane and left to rotate for 1 hr at 4°C. The resin was then pellet by centrifugation (300g, 2 mins) and resuspended in the binding buffer and transferred to a spin column (Pierce). The resin was then washed with the wash buffer (purification buffer, 0.003% GDN) to exchange detergent systems (3 washes with 4x resin volume), by gravity. The complex was then eluted off with the elution buffer (buffer system, 0.003% GDN and 150 µg/mL 3X FLAG® peptide (Merck)), 1x resin volume by gravity, 3 elutions. The elution was then concentrated with 300 kDa concentrators to remove FLAG peptide and to concentrate the protein sample required concentration.

Spectra of the purified supercomplex were collected using a cuvette system with a similar cytochrome spectroscopy setup to the bioenergetic chamber except the quartz crucible is replaced with a cuvette, allowing transmission measurements (10 mm pathlength); the volume of the cuvette is 2.1 mL. The difference spectrum was collected by subtracting the reduced spectrum (sodium dithionite) from the oxidised spectrum ($K_3[Fe(CN)_6]$).

ΔΨ and ΔpH estimates on Msm

ΔΨ and ΔpH was measured as in Rao et al (*56*) with some adjustments. Cells were prepared as for the chamber, pelleted and washed in media without Tween-80 and resuspended to an OD_{600} of 1. The cells were then split and incubated at 37°C in the 5 different conditions for 1 minute: cells alone, DMSO, bedaquiline (30 nM) and DCCD (10 mM)). This was followed by the addition of $[^3H]TPP^+$ (5 µM) and a further incubation for 1 min at 37°C. After this the cultures were centrifuged through 0.35 mL of silicon oil at 13000 x RCF for 5 mins, 22°C. 20 µL of supernatant samples were removed and the tube and rest of the contents were frozen at -80°C overnight. The frozen pellet was removed with dog nail clippers. The supernatant and the pellet were mixed with 2 mL of scintillation fluid and placed in a scintillator to measure radioactivity. $\Delta\Psi$ was estimated based on the uptake of $[^3H]TPP^+$ according

to the Nernst equation. Non-specific binding of TPP^+ was estimated from the cells that had been treated with Valinomycin.

Estimates for ZΔpH were performed side by side with $\Delta\Psi$, except [7-^{14}C]benzoate (5 µM, pKa 4.2) was added rather than [^{3}H]TPP^+ and valinomycin replaced nigericin (15 nM). ΔpH was estimated by the distribution of [7-^{14}C]benzoate using the Henderson-Hasselbalch equation. ZΔpH was calculated as $\frac{-2.3RT}{F} \times 1000 \times \Delta pH$ which approximates to $62 \times \Delta pH$. For comparisons between conditions, a repeated-measures ANOVA was conducted using JASP Version 0.19.0 (JASP Team) with a Bonferroni post-hoc test.

Conflict of interest statement

RJS is the founder of Cellspex Inc, a start-up company working to commercialise the remission spectroscopy technology used in this work.

Acknowledgements

People acknowledgements

We thank Dr Pooja Gupta (University of York), Dr Kiel Hards (University of Otago), and Dr Aneurin Kennerly (Manchester Metropolitan University) for formative discussions and Dr Matthew McNeil (University of Otago) for help with strains and microbiology. YSBL technicians and the Department of Chemistry and Biology workshops (University of York) provided critical support.

Funding acknowledgements

This work was funded by a UKRI Future Leader Fellowship to JNB (MR/T040742/1), which directly supported MMO, and the Health Research Council of New Zealand. Work in JNB's laboratory is also supported by a BBSRC sLoLa award (BB/X003035/1). SHH was supported by a Department of Chemistry teaching PhD studentship and RCW with a BBSRC White Rose PhD Studentship (2434192); RCW was also supported by a travel grant funded by a philanthropic award from Dr Tony Wild (Wild Visiting Scholars Fund).

CRediT (Contributor Roles Taxonomy)

	SHH	RCW	CYC	RJS	GMC	MMO	JNB
Conceptualization	✓	✓			✓	✓	✓
Methodology	✓	✓	✓	✓	✓	✓	✓
Software		✓		✓		✓	
Validation	✓	✓		✓		✓	✓
Formal analysis		✓		✓		✓	✓
Investigation	✓	✓	✓			✓	
Resources				✓	✓	✓	
Data Curation	✓	✓				✓	✓
Writing - original draft	✓	✓				✓	✓
Writing - review and editing	✓	✓	✓	✓	✓	✓	✓
Visualisation	✓	✓				✓	✓
Supervision					✓	✓	✓
Project administration					✓		✓
Funding acquisition					✓		✓

References

1. "Global Tuberculosis Report 2023" (World Health Organization, Geneva, 2023).
2. B.-T. Nyang'wa, C. Berry, E. Kazounis, I. Motta, N. Parpieva, Z. Tigay, V. Solodovnikova, I. Liverko, R. Moodliar, M. Dodd, N. Ngubane, M. Rassool, T. D. McHugh, M. Spigelman, D. A. J. Moore, K. Ritmeijer, P. Du Cros, K. Fielding, A 24-Week, All-Oral Regimen for Rifampin-Resistant Tuberculosis. *N. Engl. J. Med.* **387**, 2331–2343 (2022).
3. F. Conradie, T. R. Bagdasaryan, S. Borisov, P. Howell, L. Mikiashvili, N. Ngubane, A. Samoilova, S. Skornykova, E. Tudor, E. Variava, P. Yablonskiy, D. Everitt, G. H. Wills, E. Sun, M. Olugbosi, E. Egizi, M. Li, A. Holsta, J. Timm, A. Bateson, A. M. Crook, S. M. Fabiane, R. Hunt, T. D. McHugh, C. D. Tweed, S. Foraida, C. M. Mendel, M. Spigelman, Bedaquiline–Pretomanid–Linezolid Regimens for Drug-Resistant Tuberculosis. *N. Engl. J. Med.* **387**, 810–823 (2022).
4. B. Derendinger, A. Dippenaar, M. De Vos, S. Huo, R. Alberts, R. Tadokera, J. Limberis, F. Sirgel, T. Dolby, C. Spies, A. Reuter, M. Folkerts, C. Allender, D. Lemmer, A. Van Rie, S. Gagneux, L. Rigouts, J. Te Riele, K. Dheda, D. M. Engelthaler, R. Warren, J. Metcalfe, H. Cox, G. Theron, Bedaquiline resistance in patients with drug-resistant tuberculosis in Cape Town, South Africa: a retrospective longitudinal cohort study. *Lancet Microbe* **4**, e972–e982 (2023).
5. K. Hards, C. Adolph, L. K. Harold, M. B. McNeil, C.-Y. Cheung, A. Jinich, K. Y. Rhee, G. M. Cook, Two for the price of one: Attacking the energetic-metabolic hub of mycobacteria to produce new chemotherapeutic agents. *Prog. Biophys. Mol. Biol.* **152**, 35–44 (2020).
6. K. Andries, P. Verhasselt, J. Guillemont, H. W. H. Göhlmann, J.-M. Neefs, H. Winkler, J. Van Gestel, P. Timmerman, M. Zhu, E. Lee, P. Williams, D. de Chaffoy, E. Huitric, S. Hoffner, E. Cambau, C. Truffot-Pernot, N. Lounis, V. Jarlier, A diarylquinoline drug active on the ATP synthase of *Mycobacterium tuberculosis*. *Science* **307**, 223–227 (2005).
7. A. Koul, N. Dendouga, K. Vergauwen, B. Molenberghs, L. Vranckx, R. Willebrords, Z. Ristic, H. Lill, I. Dorange, J. Guillemont, D. Bald, K. Andries, Diarylquinolines target subunit c of mycobacterial ATP synthase. *Nat. Chem. Biol.* **3**, 323–324 (2007).
8. L. Preiss, J. D. Langer, Ö. Yildiz, L. Eckhardt-Strelau, J. E. G. Guillemont, A. Koul, T. Meier, Structure of the mycobacterial ATP synthase F_o rotor ring in complex with the anti-TB drug bedaquiline. *Sci. Adv.* **1**, e1500106 (2015).
9. H. Guo, G. M. Courbon, S. A. Bueler, J. Mai, J. Liu, J. L. Rubinstein, Structure of mycobacterial ATP synthase bound to the tuberculosis drug bedaquiline. *Nature* **589**, 143–147 (2021).
10. Y. Zhang, Y. Lai, S. Zhou, T. Ran, Y. Zhang, Z. Zhao, Z. Feng, L. Yu, J. Xu, K. Shi, J. Wang, Y. Pang, L. Li, H. Chen, L. W. Guddat, Y. Gao, F. Liu, Z. Rao, H. Gong, Inhibition of M. tuberculosis and human ATP synthase by BDQ and TBAJ-587. *Nature* **631**, 409–414 (2024).
11. M. Luo, W. Zhou, H. Patel, A. P. Srivastava, J. Symersky, M. M. Bonar, J. D. Faraldo-Gómez, M. Liao, D. M. Mueller, Bedaquiline inhibits the yeast and human mitochondrial ATP synthases. *Commun. Biol.* **3**, 452 (2020).
12. A. Koul, L. Vranckx, N. Dhar, H. W. H. Göhlmann, E. Özdemir, J.-M. Neefs, M. Schulz, P. Lu, E. Mørtz, J. D. McKinney, K. Andries, D. Bald, Delayed bactericidal response of *Mycobacterium tuberculosis* to bedaquiline involves remodelling of bacterial metabolism. *Nat. Commun.* **5**, 3369 (2014).
13. J. S. Mackenzie, D. A. Lamprecht, R. Asmal, J. H. Adamson, K. Borah, D. J. V. Beste, B. S. Lee, K. Pethe, S. Rousseau, I. Krieger, J. C. Sacchettini, J. N. Glasgow, A. J. C. Steyn, Bedaquiline reprograms central metabolism to reveal glycolytic vulnerability in *Mycobacterium tuberculosis* . *Nat. Commun.* **11**, 6092 (2020).
14. D. A. Lamprecht, P. M. Finin, Md. A. Rahman, B. M. Cumming, S. L. Russell, S. R. Jonnala, J. H. Adamson, A. J. C. Steyn, Turning the respiratory flexibility of *Mycobacterium tuberculosis* against itself. *Nat. Commun.* **7**, 12393 (2016).
15. K. Hards, J. R. Robson, M. Berney, L. Shaw, D. Bald, A. Koul, K. Andries, G. M. Cook, Bactericidal mode of action of bedaquiline. *J. Antimicrob. Chemother.* **70**, 2028–2037 (2015).
16. K. Hards, D. G. G. McMillan, L. A. Schurig-Briccio, R. B. Gennis, H. Lill, D. Bald, G. M. Cook, Ionophoric effects of the antitubercular drug bedaquiline. *Proc. Natl. Acad. Sci.* **115**, 7326–7331 (2018).

17. S. A. Harden, G. M. Courbon, Y. Liang, A. S. Kim, J. L. Rubinstein, A simple assay for inhibitors of mycobacterial oxidative phosphorylation. *J. Biol. Chem.* **300**, 105483 (2024).
18. M. Berney, T. E. Hartman, W. R. Jacobs, A *Mycobacterium tuberculosis* Cytochrome *bd* Oxidase Mutant Is Hypersensitive to Bedaquiline. *mBio* **5**, e01275-14 (2014).
19. N. Kim, M. O. Ripple, R. Springett, Measurement of the Mitochondrial Membrane Potential and pH Gradient from the Redox Poise of the Hemes of the bc_1 Complex. *Biophys. J.* **102**, 1194–1203 (2012).
20. Y. Liang, A. Plourde, S. A. Bueler, J. Liu, P. Brzezinski, S. Vahidi, J. L. Rubinstein, Structure of mycobacterial respiratory complex I. *Proc. Natl. Acad. Sci.* **120**, e2214949120 (2023).
21. H. Gong, Y. Gao, X. Zhou, Y. Xiao, W. Wang, Y. Tang, S. Zhou, Y. Zhang, W. Ji, L. Yu, C. Tian, S. M. Lam, G. Shui, L. W. Guddat, L.-L. Wong, Q. Wang, Z. Rao, Cryo-EM structure of trimeric *Mycobacterium smegmatis* succinate dehydrogenase with a membrane-anchor SdhF. *Nat. Commun.* **11**, 4245 (2020).
22. X. Zhou, Y. Gao, W. Wang, X. Yang, X. Yang, F. Liu, Y. Tang, S. M. Lam, G. Shui, L. Yu, C. Tian, L. W. Guddat, Q. Wang, Z. Rao, H. Gong, Architecture of the mycobacterial succinate dehydrogenase with a membrane-embedded Rieske FeS cluster. *Proc. Natl. Acad. Sci.* **118**, e2022308118 (2021).
23. W. Wang, Y. Gao, Y. Tang, X. Zhou, Y. Lai, S. Zhou, Y. Zhang, X. Yang, F. Liu, L. W. Guddat, Q. Wang, Z. Rao, H. Gong, Cryo-EM structure of mycobacterial cytochrome *bd* reveals two oxygen access channels. *Nat. Commun.* **12**, 4621 (2021).
24. S. Safarian, H. K. Opel-Reading, D. Wu, A. R. Mehdipour, K. Hards, L. K. Harold, M. Radloff, I. Stewart, S. Welsch, G. Hummer, G. M. Cook, K. L. Krause, H. Michel, The cryo-EM structure of the *bd* oxidase from *M. tuberculosis* reveals a unique structural framework and enables rational drug design to combat TB. *Nat. Commun.* **12**, 5236 (2021).
25. D. Riepl, A. P. Gamiz-Hernandez, T. Kovalova, S. M. Król, S. L. Mader, D. Sjöstrand, M. Högbom, P. Brzezinski, V. R. I. Kaila, Long-range charge transfer mechanism of the III_2IV_2 mycobacterial supercomplex. *Nat. Commun.* **15**, 5276 (2024).
26. H. Gong, J. Li, A. Xu, Y. Tang, W. Ji, R. Gao, S. Wang, L. Yu, C. Tian, J. Li, H.-Y. Yen, S. Man Lam, G. Shui, X. Yang, Y. Sun, X. Li, M. Jia, C. Yang, B. Jiang, Z. Lou, C. V. Robinson, L.-L. Wong, L. W. Guddat, F. Sun, Q. Wang, Z. Rao, An electron transfer path connects subunits of a mycobacterial respiratory supercomplex. *Science* **362**, eaat8923 (2018).
27. B. Wiseman, R. G. Nitharwal, O. Fedotovskaya, J. Schäfer, H. Guo, Q. Kuang, S. Benlekbir, D. Sjöstrand, P. Ädelroth, J. L. Rubinstein, P. Brzezinski, M. Högbom, Structure of a functional obligate complex III_2IV_2 respiratory supercomplex from *Mycobacterium smegmatis*. *Nat. Struct. Mol. Biol.* **25**, 1128–1136 (2018).
28. V. P. Shinkarev, A. R. Crofts, C. A. Wraight, Spectral analysis of the bc_1 complex components in situ: Beyond the traditional difference approach. *Biochim. Biophys. Acta BBA - Bioenerg.* **1757**, 67–77 (2006).
29. N. Kim, M. O. Ripple, R. Springett, Spectral components of the α-band of cytochrome oxidase. *Biochim. Biophys. Acta BBA - Bioenerg.* **1807**, 779–787 (2011).
30. V. P. Shinkarev, A. R. Crofts, C. A. Wraight, The Electric Field Generated by Photosynthetic Reaction Center Induces Rapid Reversed Electron Transfer in the bc_1 Complex. *Biochemistry* **40**, 12584–12590 (2001).
31. B. S. Lee, K. Hards, C. A. Engelhart, E. J. Hasenoehrl, N. P. Kalia, J. S. Mackenzie, E. Sviriaeva, S. M. S. Chong, M. S. S. Manimekalai, V. H. Koh, J. Chan, J. Xu, S. Alonso, M. J. Miller, A. J. C. Steyn, G. Grüber, D. Schnappinger, M. Berney, G. M. Cook, G. C. Moraski, K. Pethe, Dual inhibition of the terminal oxidases eradicates antibiotic‐tolerant *Mycobacterium tuberculosis*. *EMBO Mol. Med.* **13**, e13207 (2021).
32. X. Lu, Z. Williams, K. Hards, J. Tang, C.-Y. Cheung, H. L. Aung, B. Wang, Z. Liu, X. Hu, A. Lenaerts, L. Woolhiser, C. Hastings, X. Zhang, Z. Wang, K. Rhee, K. Ding, T. Zhang, G. M. Cook, Pyrazolo[1,5- *a*]pyridine Inhibitor of the Respiratory Cytochrome *bcc* Complex for the Treatment of Drug-Resistant Tuberculosis. *ACS Infect. Dis.* **5**, 239–249 (2019).
33. V. B. Borisov, R. B. Gennis, J. Hemp, M. I. Verkhovsky, The cytochrome bd respiratory oxygen reductases. *Biochim. Biophys. Acta BBA - Bioenerg.* **1807**, 1398–1413 (2011).
34. P. Chauhan, S. A. Van Der Meulen, J. M. Simões Caetano, H. G. Goojani, D. Botman, R. Van

Spanning, H. Lill, D. Bald, Response of *Mycobacterium smegmatis* to the Cytochrome *bcc* Inhibitor Q203. *Int. J. Mol. Sci.* **23**, 10331 (2022).
35. R. C. Hartkoorn, S. Uplekar, S. T. Cole, Cross-Resistance between Clofazimine and Bedaquiline through Upregulation of MmpL5 in Mycobacterium tuberculosis. *Antimicrob. Agents Chemother.* **58**, 2979–2981 (2014).
36. A. Giraud-Gatineau, J. M. Coya, A. Maure, A. Biton, M. Thomson, E. M. Bernard, J. Marrec, M. G. Gutierrez, G. Larrouy-Maumus, R. Brosch, B. Gicquel, L. Tailleux, The antibiotic bedaquiline activates host macrophage innate immune resistance to bacterial infection. *eLife* **9**, e55692 (2020).
37. R. P. G. Van Heeswijk, B. Dannemann, R. M. W. Hoetelmans, Bedaquiline: a review of human pharmacokinetics and drug-drug interactions. *J. Antimicrob. Chemother.* **69**, 2310–2318 (2014).
38. D. J. Greenwood, M. S. Dos Santos, S. Huang, M. R. G. Russell, L. M. Collinson, J. I. MacRae, A. West, H. Jiang, M. G. Gutierrez, Subcellular antibiotic visualization reveals a dynamic drug reservoir in infected macrophages. *Science* **364**, 1279–1282 (2019).
39. M. Rocha, R. Springett, Measuring the functionality of the mitochondrial pumping complexes with multi-wavelength spectroscopy. *Biochim. Biophys. Acta BBA - Bioenerg.* **1860**, 89–101 (2019).
40. N. P. Kalia, S. Singh, K. Hards, C.-Y. Cheung, E. Sviriaeva, A. Banaei-Esfahani, R. Aebersold, M. Berney, G. M. Cook, K. Pethe, *M. tuberculosis* relies on trace oxygen to maintain energy homeostasis and survive in hypoxic environments. *Cell Rep.* **42**, 112444 (2023).
41. L. E. Via, P. L. Lin, S. M. Ray, J. Carrillo, S. S. Allen, S. Y. Eum, K. Taylor, E. Klein, U. Manjunatha, J. Gonzales, E. G. Lee, S. K. Park, J. A. Raleigh, S. N. Cho, D. N. McMurray, J. L. Flynn, C. E. Barry, Tuberculous Granulomas Are Hypoxic in Guinea Pigs, Rabbits, and Nonhuman Primates. *Infect. Immun.* **76**, 2333–2340 (2008).
42. T. Beites, K. O'Brien, D. Tiwari, C. A. Engelhart, S. Walters, J. Andrews, H.-J. Yang, M. L. Sutphen, D. M. Weiner, E. K. Dayao, M. Zimmerman, B. Prideaux, P. V. Desai, T. Masquelin, L. E. Via, V. Dartois, H. I. Boshoff, C. E. Barry, S. Ehrt, D. Schnappinger, Plasticity of the Mycobacterium tuberculosis respiratory chain and its impact on tuberculosis drug development. *Nat. Commun.* **10**, 4970 (2019).
43. Y. Cai, E. Jaecklein, J. S. Mackenzie, K. Papavinasasundaram, A. J. Olive, X. Chen, A. J. C. Steyn, C. M. Sassetti, Host immunity increases *Mycobacterium tuberculosis* reliance on cytochrome *bd* oxidase. *PLOS Pathog.* **17**, e1008911 (2021).
44. A. Gouzy, C. Healy, K. A. Black, K. Y. Rhee, S. Ehrt, Growth of *Mycobacterium tuberculosis* at acidic pH depends on lipid assimilation and is accompanied by reduced GAPDH activity. *Proc. Natl. Acad. Sci.* **118**, e2024571118 (2021).
45. T. Q. Nguyen, B. T. B. Hanh, S. Jeon, B. E. Heo, Y. Park, A. Choudhary, C. Moon, J. Jang, Synergistic Effect of Q203 Combined with PBTZ169 against Mycobacterium tuberculosis. *Antimicrob. Agents Chemother.* **66**, e00448-22 (2022).
46. W. Yu, Y. Ju, X. Han, X. Tian, J. Ding, S. Wang, H. M. A. Hameed, Y. Gao, L. Li, Y. Li, N. Zhong, T. Zhang, Bactericidal and sterilizing activity of sudapyridine-clofazimine-TB47 combined with linezolid or pyrazinamide in a murine model of tuberculosis. *Antimicrob. Agents Chemother.*, e00124-24 (2024).
47. L. N. Jeffreys, A. Ardrey, T. A. Hafiz, L.-A. Dyer, A. J. Warman, N. Mosallam, G. L. Nixon, N. E. Fisher, W. D. Hong, S. C. Leung, G. Aljayyoussi, J. Bibby, D. V. Almeida, P. J. Converse, N. Fotouhi, N. G. Berry, E. L. Nuermberger, A. M. Upton, P. M. O'Neill, S. A. Ward, G. A. Biagini, Identification of 2-Aryl-Quinolone Inhibitors of Cytochrome *bd* and Chemical Validation of Combination Strategies for Respiratory Inhibitors against *Mycobacterium tuberculosis*. *ACS Infect. Dis.* **9**, 221–238 (2023).
48. K. Williams, A. Minkowski, O. Amoabeng, C. A. Peloquin, D. Taylor, K. Andries, R. S. Wallis, K. E. Mdluli, E. L. Nuermberger, Sterilizing Activities of Novel Combinations Lacking First- and Second-Line Drugs in a Murine Model of Tuberculosis. *Antimicrob. Agents Chemother.* **56**, 3114–3120 (2012).
49. T. Yano, S. Kassovska-Bratinova, J. S. Teh, J. Winkler, K. Sullivan, A. Isaacs, N. M. Schechter, H. Rubin, Reduction of Clofazimine by Mycobacterial Type 2 NADH:Quinone Oxidoreductase. *J. Biol. Chem.* **286**, 10276–10287 (2011).

50. R. Benz, S. McLaughlin, The molecular mechanism of action of the proton ionophore FCCP (carbonylcyanide p-trifluoromethoxyphenylhydrazone). *Biophys. J.* **41**, 381–398 (1983).
51. K. R. Pryde, J. Hirst, Superoxide Is Produced by the Reduced Flavin in Mitochondrial Complex I. *J. Biol. Chem.* **286**, 18056–18065 (2011).
52. V. K. Sambandamurthy, S. C. Derrick, T. Hsu, B. Chen, M. H. Larsen, K. V. Jalapathy, M. Chen, J. Kim, S. A. Porcelli, J. Chan, S. L. Morris, W. R. Jacobs, *Mycobacterium tuberculosis* Δ*RD1* Δ*panCD*: A safe and limited replicating mutant strain that protects immunocompetent and immunocompromised mice against experimental tuberculosis. *Vaccine* **24**, 6309–6320 (2006).
53. M. C. Whitlock, Dolph Schluter, *The Analysis of Biological Data* (Macmillan International, Third., 2020).
54. D. J. Yanofsky, J. M. Di Trani, S. Król, R. Abdelaziz, S. A. Bueler, P. Imming, P. Brzezinski, J. L. Rubinstein, Structure of mycobacterial $CIII_2CIV_2$ respiratory supercomplex bound to the tuberculosis drug candidate telacebec (Q203). *eLife* **10**, e71959 (2021).
55. K. C. Murphy, S. J. Nelson, S. Nambi, K. Papavinasasundaram, C. E. Baer, C. M. Sassetti, ORBIT: a New Paradigm for Genetic Engineering of Mycobacterial Chromosomes. *mBio* **9**, e01467-18 (2018).
56. M. Rao, T. L. Streur, F. E. Aldwell, G. M. Cook, Intracellular pH regulation by *Mycobacterium smegmatis* and *Mycobacterium bovis* BCG. *Microbiology* **147**, 1017–1024 (2001).